

# An Intrinsically Antifreezing and Self-Adhesive Hydrogel Electrolyte for Flexible Zinc Ion Hybrid Capacitors

Zenghao Li,<sup>[a, b]</sup> Yujing Sheng,<sup>[a, b]</sup> Xingfa Gao,<sup>[b, c]</sup> Yuzhen Huang,<sup>[b, c]</sup> Zhenzhong Han,<sup>\*[d]</sup> Ruliang Zhang,<sup>\*[a]</sup> and Yinglun Sun<sup>\*[b, c]</sup>

Flexible zinc ion hybrid capacitors (ZIHCs) have attracted extensive research interest by virtue of their high safety and low cost. However, their low-temperature application remains limited due to the freeze of hydrogel electrolytes. Herein, we prepared an intrinsically antifreezing amphiphilic copolymer hydrogel based on hydrophilic monomer 2-Hydroxyethyl acrylate and hydrophobic monomer 1H, 1H, 2H, 2H perfluorooctyl methacrylate. Thanks to the hydrogen bond destruction effect of the hydrophilic units and the nano-confinement effect of the hydrophobic units, the hydrogel exhibited a freezing

point as low as  $-30^{\circ}\text{C}$ , which was significantly lower than that of hydrogel prepared using pure hydrophilic monomers. In addition, the hydrogel also showed excellent adhesion performance, which contributed to the assembly of device and prevented layer-to-layer slippage during the device use. By soaking the hydrogel in  $\text{Zn}(\text{ClO}_4)_2$  solution to serve as the electrolyte of the ZIHC, the device achieved excellent electrochemical performance at  $-50^{\circ}\text{C}$ . This work provides a new path for the design of antifreeze hydrogel electrolytes for ZIHCs.

## Introduction

Zinc ion hybrid capacitors (ZIHCs), a new type of hybrid supercapacitor, have gained significant attention due to their combination of high power density, a characteristic of supercapacitors, and high energy density, similar to zinc-ion batteries.<sup>[1–4]</sup> In addition, ZIHCs utilize aqueous electrolytes, offering advantages such as high safety and low cost.<sup>[5–7]</sup> Therefore, these attributes make ZIHCs highly promising for wearable medical devices. However, for practical application as electrochemical energy storage devices, ZIHCs must operate in low-temperature environments. For example, outdoor temperatures in northern China during the winter generally drop

below  $0^{\circ}\text{C}$ , with the average lowest temperature in northeastern China even reaching  $-30^{\circ}\text{C}$ .<sup>[8]</sup> Real-time health monitoring in such extreme conditions is critical for preventing cardiovascular disease, which has the highest mortality rate. Consequently, beyond improving the room-temperature energy density and cycle life of ZIHCs, it is necessary to develop low-temperature flexible ZIHCs to meet the low-temperature application requirements of future wearable devices.

A key factor limiting the normal operation of flexible ZIHCs at low temperatures is the electrolyte.<sup>[9–11]</sup> Gel electrolytes used in flexible ZIHCs contain zinc salt aqueous solutions, such as  $\text{ZnSO}_4$  and  $\text{Zn}[\text{CF}_3\text{SO}_3]_2$  solutions.<sup>[12]</sup> The water solvent with a high freezing point causes these hydrogel electrolytes to easily freeze below  $0^{\circ}\text{C}$ , resulting in a sudden drop in the ionic conductivity of hydrogel electrolytes, which would cause a decline in the performance of ZIHCs or even device failure.<sup>[13]</sup> The fundamental reason for the freeze of hydrogel electrolytes at low temperatures involves hydrogen bond interactions between water molecules, which can be significantly enhanced at temperatures below zero, eventually leading to the formation of a three-dimensional hydrogen bond network.<sup>[14]</sup> Therefore, to inhibit the freeze of hydrogel electrolytes, it is necessary to inhibit hydrogen bond interactions between water molecules.<sup>[15]</sup> A common strategy involves adding organic solvents to hydrogel electrolytes.<sup>[16–18]</sup> For example, Zhang et al. introduced ethylene glycol to polyvinyl alcohol (PVA) to prepare an antifreeze hydrogel electrolyte, and the assembled ZIHC exhibited excellent electrochemical performance at  $-15^{\circ}\text{C}$ .<sup>[19]</sup> Although the introduction of organic solvents can significantly depress the freezing point of hydrogel electrolytes, the organic additives would seriously reduce the solubility of salts in the hydrogel electrolytes, resulting in a reduction in the ionic conductivity of hydrogel electrolytes.<sup>[20]</sup> Another commonly used strategy involves increasing the concentration of salts in hydrogel electrolytes.<sup>[21–23]</sup> For example, Li et al. added

[a] Z. Li, Y. Sheng, R. Zhang  
School of Materials Science and Engineering, Shandong University of Science and Technology  
Qingdao 266590, China  
E-mail: rlzhit@126.com

[b] Z. Li, Y. Sheng, X. Gao, Y. Huang, Y. Sun  
Institute of Medical Engineering and Interdisciplinary Research, Medical Science and Technology Innovation Center, Shandong First Medical University & Shandong Academy of Medical Sciences  
Jinan 250117, China  
E-mail: sunyinglun@sdfmu.edu.cn

[c] X. Gao, Y. Huang, Y. Sun  
Medical Engineering and Technology Research Center, School of Radiology, Shandong First Medical University & Shandong Academy of Medical Sciences  
Taian 271016, China

[d] Z. Han  
Biomedical Sciences College & Shandong Medicinal Biotechnology Centre, Shandong First Medical University & Shandong Academy of Medical Sciences  
Jinan 250117, China  
E-mail: zhonghuijue@163.com

 Supporting information for this article is available on the WWW under <https://doi.org/10.1002/batt.202500026>

15 mol L<sup>-1</sup> NaClO<sub>4</sub> to a double-network hydrogel and obtained a freezing point of  $-40^{\circ}\text{C}$ .<sup>[24]</sup> However, increasing the additional salt concentration can lead to an increase in the cost of hydrogel electrolytes.<sup>[25]</sup> Therefore, it is necessary to develop new antifreeze strategies to address the current issues of hydrogel electrolytes.

In our previous work, we found that a gel electrolyte prepared with hydrophilic PVA as the matrix exhibited a lower freezing point than the corresponding aqueous solution, indicating that the introduction of PVA could reduce the freezing point of the aqueous solution.<sup>[26]</sup> This was because PVA chains could form hydrogen bonds with the water molecules, disrupting the hydrogen bond interactions between the water molecules. However, the effect of inhibiting the freeze of the gel electrolyte could only be achieved until  $-20^{\circ}\text{C}$ . Vogt et al. found that water molecules could be restricted in the nanoscale range of hydrogels by hydrophobic segments, thereby suppressing the freeze of water.<sup>[27]</sup> For example, hydrophobic nanodomains were found to form in the copolymer hydrogel based on dimethylacrylamide and 2-(N-ethylperfluorooctane sulfonamido) ethyl acrylate through hydrophobic supramolecular assembly, providing a solid soft constraint environment for the water molecules, preventing 45 wt% of the water in the hydrogel from crystallizing.<sup>[27]</sup> In this case, polymerizing hydrophilic polymer and hydrophobic polymer monomers to form amphiphilic copolymers could enhance the inhibition of water crystallization. Recent experimental result obtained by Vogt et al. demonstrated that replacing dimethylacrylamide with 2-hydroxyethyl acrylate and polymerizing it with 2-(N-ethylperfluorooctane sulfonamido) ethyl acrylate to prepare amphiphilic copolymers could significantly depress the freezing point of the hydrogels.<sup>[28]</sup> However, amphiphilic copolymer hydrogels have not yet been reported for low-temperature flexible ZIHCs.

In this work, we synthesized an amphiphilic copolymer hydrogel via the free radical polymerization of the hydrophilic monomer 2-hydroxyethyl acrylate (HEA) and the hydrophobic monomer 1H, 1H, 2H, 2H perfluoroctyl methacrylate (PFM). The amphiphilic hydrogel exhibited a freezing point as low as  $-30^{\circ}\text{C}$ , which was lower than that of the hydrogel prepared using a single hydrophilic monomer. This was mainly because the hydrophilic units in the hydrogel could interact with water molecules to disrupt the hydrogen bond interactions between the water molecules, and the confinement effect of hydrophobic units on water molecules limited the movement of water molecules. In addition, the excellent adhesion performance of the amphiphilic hydrogel significantly promoted contact between the electrolyte and the electrode, which was conducive to the uniform deposition of Zn<sup>2+</sup> ions and rapid ion transport. The electrolyte prepared by immersing the hydrogel in the Zn(ClO<sub>4</sub>)<sub>2</sub> aqueous solution enabled the ZIHC to operate normally at  $-50^{\circ}\text{C}$  and obtain excellent electrochemical performance.

## Results and Discussion

The preparation process of the amphiphilic copolymer hydrogel is illustrated in Figure 1a. The amphiphilic copolymer hydrogel was synthesized through free radical polymerization, then the amphiphilic copolymer was immersed in water to obtain the hydrogel. Due to hydrogen bond interactions between the hydrophilic segments and entanglement between the hydrophobic long chains, the polymer network was obtained by physical cross-linking. For the convenience of the following description, the amphiphilic copolymer was denoted as HF<sub>x</sub>, with H representing hydrophilic monomer HEA, F representing hydrophobic monomer PFM, and x representing the molar ratio of the hydrophobic monomers. The chemical structure of the HF copolymers was determined through nuclear magnetic resonance (NMR) characterization. HEA and PFM exhibited C=C peaks at  $\delta=5.8\text{--}6.4$  and  $5.6\text{--}6.2$ , respectively, while the C=C peak was not detected in the HF copolymer, indicating the successful polymerization of HEA and PFM. The molar ratio of HEA to PFM in the HF copolymer was determined by <sup>1</sup>H NMR spectroscopy and calculating the area ratios of methylene (CH<sub>2</sub>,  $\delta=3.6\text{--}3.9$ ) in HEA and methyl (CH<sub>3</sub>,  $\delta=0.9\text{--}1.2$ ) in PFM. Figure 1c presents the <sup>1</sup>H NMR spectra of the HF copolymers with different molar ratios, illustrating the chemical structure of the HF copolymers. Synthesis of the HF copolymer was also confirmed by Fourier transform infrared spectroscopy (FTIR). As shown in Figures 1d and S1, compared with the C=C stretching vibration peaks of HEA and PFM at  $1620\text{--}1670\text{ cm}^{-1}$ , the C=C stretching vibration peak disappeared in the HF copolymers, verifying their successful synthesis. The microstructure of the HF hydrogels was also characterized by scanning electron microscopy (SEM), which indicated that the HF hydrogels contained a porous structure (Figures 1e, 1f, and S2). This structure was conducive to rapid ion diffusion, and the hydrophobic monomer contents had little effect on the morphology of the hydrogels.

As described in previous research, the addition of hydrophobic monomers can limit the movement of water molecules, thereby depressing the freezing point of hydrogels.<sup>[27,28]</sup> To verify the effect of hydrophobic monomers on water crystallization in the HF hydrogel, differential scanning calorimetry (DSC) was used to detect the freezing point of HF hydrogels with different molar ratios. Compared with the hydrophilic monomer polymer, denoted as XLHEA, the exothermic peak of the HF hydrogel shifted to a lower temperature with increasing PFM content, as shown in Figure 2a. This indicates that the addition of the hydrophobic monomer effectively reduced the freezing point of HF hydrogels. Except for hydrogen bond interactions between the hydrophilic chains and water molecules, the hydrophobic units could form nano-confinement by interlocking of hydrophobic chains, restricting the activity of water molecules and hindering the ordered arrangement of water molecules.<sup>[28]</sup> To verify this, FTIR analysis was employed to assess HF hydrogels with different molar ratios. Figure 2b and S3 presents the O–H stretching vibrations of the HF hydrogels with different molar ratios. With an increase in hydrophobic monomer content, the O–H stretching vibration peak exhibited

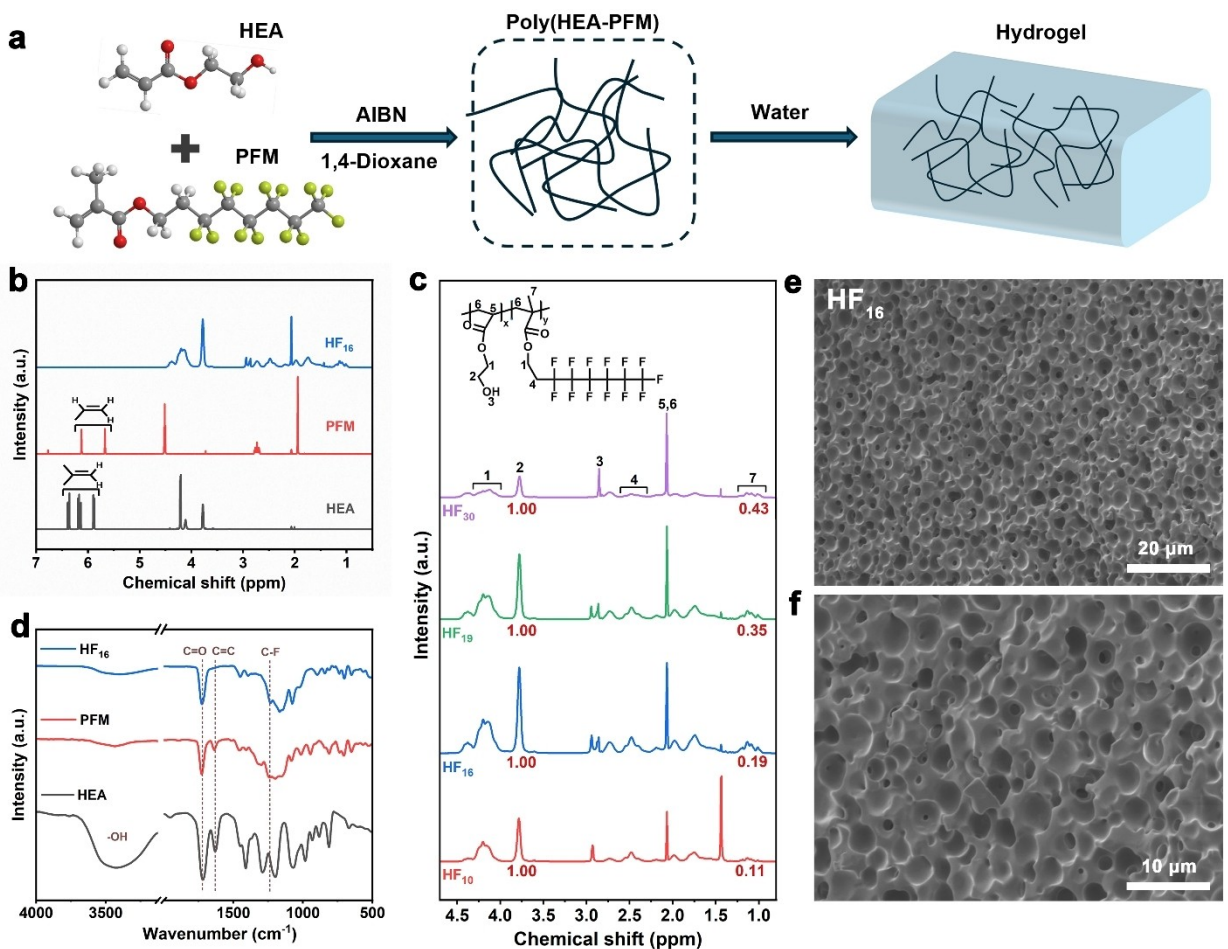


**Figure 1.** (a) Schematic diagram showing the preparation process of the amphiphilic copolymer hydrogel. (b) <sup>1</sup>H NMR spectra of HEA, PFM, and HF<sub>16</sub> copolymer. (c) <sup>1</sup>H NMR spectra of HF copolymers with different molar ratios. (d) FTIR spectra of HEA, PFM, and HF<sub>16</sub> copolymer. (e) and (f) SEM images of the HF<sub>16</sub> hydrogel.

a slight blue shift, indicating an increase in the proportion of weak hydrogen bonds.<sup>[29]</sup> In addition, we found that the peak at 3220 cm<sup>-1</sup> weakened with an increasing proportion of hydrophobic monomer. According to previous studies, the peaks at 3220, 3410, and 3570 cm<sup>-1</sup> corresponded to strong hydrogen, medium hydrogen, and weak hydrogen bonds, respectively.<sup>[30,31]</sup> By calculating the area of the fitted peak, the proportion changes of different hydrogen bonds could be obtained. With an increase in hydrophobic monomer content, the strong hydrogen bonds gradually decreased, while weak hydrogen bonds increased (Figure 3c), indicating that the nano-confinement effect formed by the hydrophobic units significantly disrupted water crystallization.

HF hydrogel electrolytes were obtained by soaking the HF amphiphilic copolymer in 1 mol kg<sup>-1</sup> Zn(ClO<sub>4</sub>)<sub>2</sub> aqueous solution. The reason for choosing Zn(ClO<sub>4</sub>)<sub>2</sub> salt as electrolyte salt is that Zn(ClO<sub>4</sub>)<sub>2</sub> aqueous solution has better low-temperature performance than other Zn salt solutions, such as ZnSO<sub>4</sub> solution, ZnCl<sub>2</sub> solution.<sup>[2]</sup> The tensile properties of HF hydrogel electrolytes and the XLHEA hydrogel electrolyte are shown in Figure S4. The XLHEA hydrogel electrolyte exhibited relatively low tensile strength. The addition of hydrophobic monomers

enhanced the tensile strength of the hydrogel electrolytes, and with an increase in hydrophobic monomers, the tensile strength of the HF hydrogel electrolyte gradually increased. When the molar ratio of the hydrophobic monomer reached 19%, the hydrogel electrolyte achieved a maximum elongation at a break of 1400% (Figure S4). However, with a further increase in hydrophobic monomer, the tensile strength of the HF hydrogel electrolyte decreased, due to the increased brittleness of the HF hydrogel electrolyte caused by excessive hydrophobic monomer content. Notably, although the tensile properties of HF hydrogel electrolytes were not unsatisfactory, they showed superior adhesion properties, which was conducive to the assembly of flexible electrochemical energy storage devices.<sup>[32]</sup> A schematic diagram of the adhesion test for the hydrogel electrolytes is shown in Figure 2d. As depicted in Figures 2e and S5, compared with the XLHEA hydrogel electrolyte, amphiphilic copolymer hydrogel electrolytes could obtain significantly enhanced adhesion performance. As the proportion of hydrophobic monomers increased, the adhesion strength gradually increased. When the proportion of hydrophobic monomer reached 19%, the adhesion strength achieved a maximum value of 55 KPa. However, excessive hydrophobic

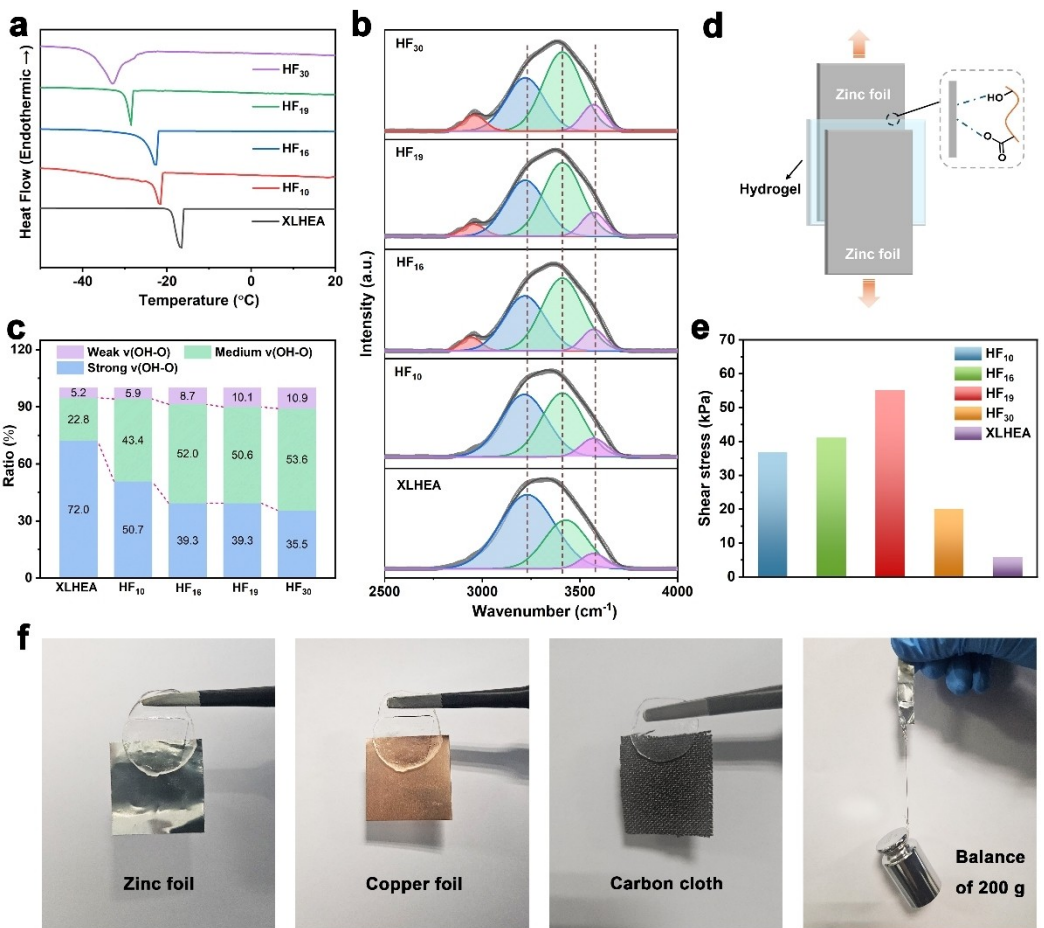


**Figure 2.** (a) DSC curves of HF hydrogels with different molar ratios and the XLHEA hydrogel. (b) FTIR spectra and (c) corresponding hydrogen bond distributions in HF hydrogels with different molar ratios and the XLHEA hydrogel. (d) Schematic diagram of adhesion performance testing. (e) Adhesion performance of HF hydrogel electrolytes with different molar ratios and the XLHEA hydrogel. (f) Digital photograph of the HF hydrogel electrolyte adhered to various substrates.

monomers not only reduced the swelling degree of HF copolymers but also weakened the hydrogen bond interactions between the hydrophilic chains and the stretched substrates, resulting in a decrease in the adhesive force between the HF hydrogel and the substrate. Moreover, the HF hydrogel could adhere to various substrates, such as copper (Cu) foil, zinc (Zn) foil, and carbon cloth. As a result, a 200 g weight could easily be lifted by two pieces of Zn foil bonded with the HF hydrogel, ensuring firm adhesion between the HF hydrogel electrolyte and the electrodes.

A Tafel test was performed to examine the corrosion behavior of different molar ratios of the HF hydrogel electrolytes on the Zn anode. As shown in Figure 3a, the hydrophobic monomer content had a significant impact on the corrosion of the Zn anode. As the content of hydrophobic monomers increased, the corrosion current initially decreased and then increased. The HF<sub>19</sub> hydrogel electrolyte exhibited the lowest corrosion current of 0.11 μA and the highest hydrogen evolution potential. Meanwhile, the HF<sub>16</sub> hydrogel electrolyte also exhibited a low corrosion current of 0.2 μA. A low corrosion current represented a low corrosion rate,<sup>[33–35]</sup> indicating that the nano-confinement formed by the hydrophobic units could

provide higher stability and corrosion resistance for the Zn anode. The nucleation overpotential in the HF hydrogel electrolytes was measured by cyclic voltammetry (CV). Figure 3b shows the nucleation overpotential of Zn deposition on Cu foil in the HF hydrogel electrolytes with different molar ratios. The effect of hydrophobic monomer content on the nucleation overpotential exhibited a trend similar to that of the corrosion current. The HF<sub>16</sub> and HF<sub>19</sub> hydrogel electrolytes both exhibited relatively low nucleation overpotential, which contributed to uniform Zn deposition with more abundant and uniform nucleation sites. All HF hydrogel electrolytes contained a pair of redox peaks, corresponding to Zn plating/stripping.<sup>[30]</sup> The HF<sub>16</sub> and HF<sub>19</sub> hydrogel electrolytes both exhibited relatively high peak currents, indicating rapid reaction kinetics of the Zn<sup>2+</sup> ions. This was possibly due to the excellent adhesion performance of the hydrogel electrolytes, which enhanced the interfacial affinity between the hydrogel electrolyte and the Zn anode.<sup>[30]</sup> To further verify the regulation of hydrophobic monomers on Zn deposition, the diffusion and nucleation behavior of Zn<sup>2+</sup> ions in the HF hydrogel electrolytes were measured by chronoamperometry (CA). Figure 3c displays the deposition behavior of Zn<sup>2+</sup> ions in the HF hydrogel electrolytes

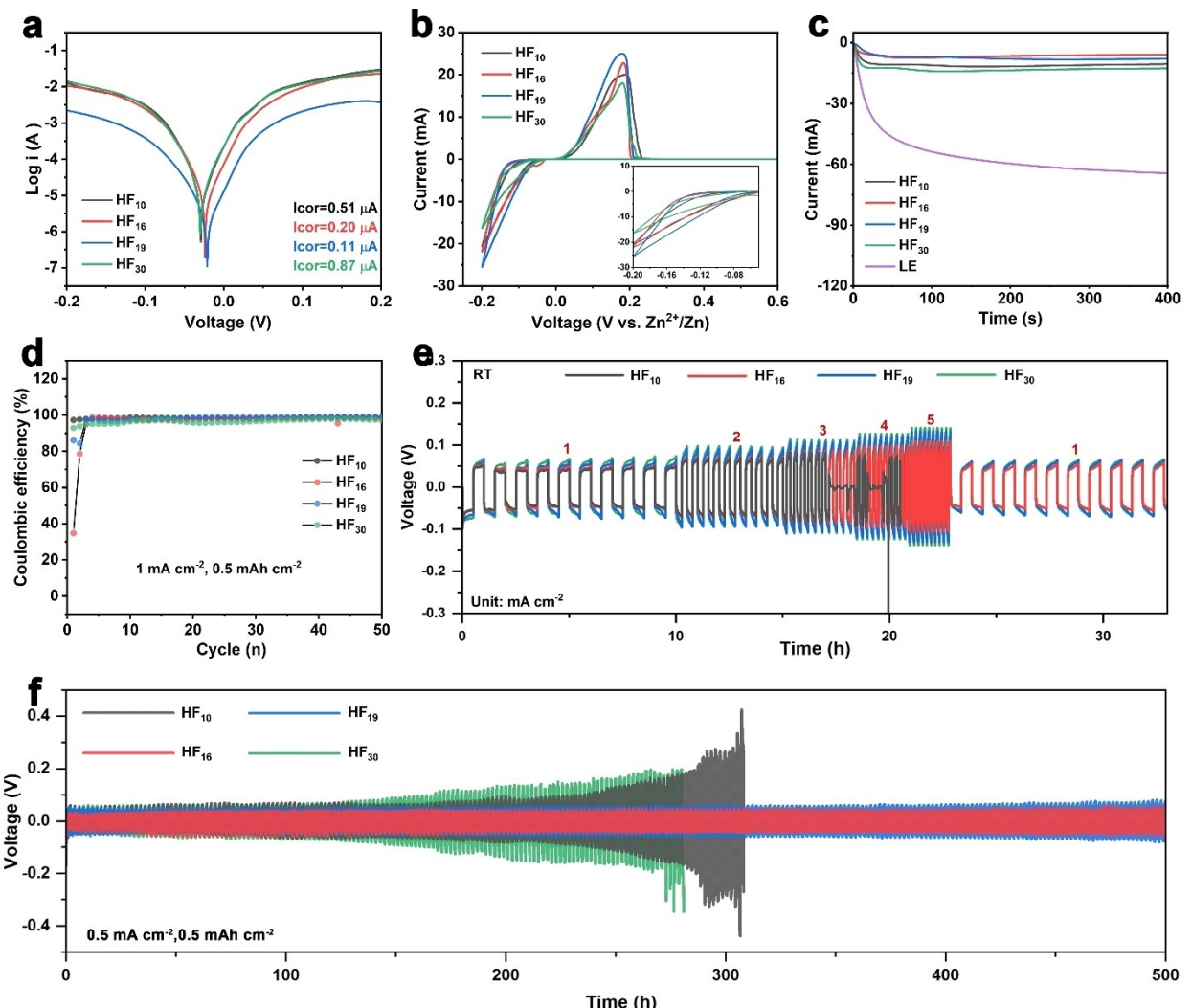


**Figure 3.** (a) Tafel curves of the Zn foil, (b) CV curves for Zn nucleation on the Cu foil, (c) CA tests, (d) Coulombic efficiency of Zn plating/stripping, (e) rate performance of Zn//Zn symmetrical cells at room temperature, and (f) cycling performance of Zn//Zn symmetrical cells at room temperature with different molar ratios of the HF hydrogel electrolytes.

with different molar ratios and liquid electrolytes. In the liquid electrolyte, the current continued to increase before 200 s, indicating that the two-dimensional diffusion of  $Zn^{2+}$  ions was not controlled, and random two-dimensional growth would exacerbate dendrite formation.<sup>[36–38]</sup> By contrast, in the HF hydrogel electrolytes, the current response with time was small, and a stable current was observed, indicating that the two-dimensional growth of  $Zn^{2+}$  ions was limited, mainly involving the three-dimensional deposition of  $Zn^{2+}$  ions, which contributed to inhibiting dendrite formation.

The reversibility of the Zn anode in HF hydrogel electrolytes with different molar ratios was assessed using Zn//Cu asymmetric cells at a current density of  $1\text{ mA cm}^{-2}$ . As shown in Figure 3d, the content of the hydrophobic monomer had minimal impact on the Coulombic efficiency of Zn plating/stripping, with all samples achieving high Coulomb efficiency above 97%. This indicated highly reversible Zn plating/stripping in the amphiphilic hydrogel electrolytes. The rate performance of the Zn//Zn symmetric cells in HF hydrogel electrolytes with

different molar ratios was also assessed. All Zn//Zn symmetric cells could maintain stable voltage profiles at all current densities, indicating superior rate performance (Figure 3e). Moreover, the cycling performance of the Zn anode in HF hydrogel electrolytes with different molar ratios was tested using Zn//Zn symmetric cells. Under a current density of  $0.5\text{ mA cm}^{-2}$  and a capacity of  $0.5\text{ mAh cm}^{-2}$  at room temperature, the  $HF_{16}$  hydrogel electrolyte and  $HF_{19}$  hydrogel electrolyte achieved a stable cycle of 500 h (Figure 3f). In addition, the  $HF_{16}$  hydrogel electrolyte exhibited a lower initial nucleation potential, indicating superior zincophilicity (Figure 3f). By contrast, an imbalance in hydrophobic monomer negatively affected the cycling performance of the Zn anode. Specifically, the Zn//Zn symmetric cell employing the  $HF_{10}$  hydrogel electrolyte began to polarize after 200 h of stable cycling, while the Zn//Zn symmetric cell employing the  $HF_{30}$  hydrogel electrolyte exhibited polarization after 150 h of stable cycling.

Considering its long cycle life and small polarization on the Zn anode, the  $HF_{16}$  hydrogel electrolyte was chosen for the

following experiments. The Coulombic efficiency of the Zn anode using the HF<sub>16</sub> hydrogel electrolyte at low temperatures was subsequently studied. Under a current density of 1 mA cm<sup>-2</sup> and a capacity of 0.5 mAh cm<sup>-2</sup>, the Coulombic efficiency ultimately reached a stable value of 98.7% after initial cycling (Figure S6), indicating the high Zn plating/stripping reversibility at low temperatures. Cycling performance tests for the Zn//Zn symmetric cell using the HF<sub>16</sub> hydrogel electrolyte at low temperatures were also conducted. As shown in Figure S7, the cell cycled stably for 700 h at -20 °C, indicating high efficiency of the Zn anode at low temperatures. To further investigate the effect of the hydrogel electrolyte on the morphology of the Zn anode, the Zn anode was characterized by SEM after 200 h of cycling. As shown in Figure S8, the Zn anode exhibited a lamellar structure without by-products at room temperature. The Zn anode after 200 h of cycling at low temperatures exhibited a similar morphology to that at room temperature. In addition, the chemical composition of the Zn anode was analyzed after 200 h of cycling using X-ray diffraction (XRD). No by-products were found after 200 h of cycling for the Zn anode at room temperature (Figure S8), confirming the SEM results. After 200 h of cycling the Zn anode at -20 °C, negligible by-products were also observed (Figure S9).

Activated carbon coating on the carbon cloth and commercial Zn foil served as the positive and negative electrodes, respectively, which were used to assemble flexible ZIHCs (Figure 4a). The room temperature electrochemical performance of the ZIHCs was examined by CV and galvanostatic charging/discharging (GCD). The CV curves of the ZIHCs using different molar ratios of HF hydrogel electrolytes with a voltage window of 0.1–1.7 V at a scan rate of 0.5 mVs<sup>-1</sup> are shown in Figure 4b. The non-ideal rectangle validated the hybrid energy storage mechanism of the ZIHCs, which involved the plating/stripping of Zn<sup>2+</sup> ions on the negative electrode and the adsorption/desorption of anions and Zn<sup>2+</sup> ions on the positive electrode.<sup>[39]</sup> The CV curves of ZIHCs all exhibited a pair of redox peaks, attributed to the plating/stripping of Zn<sup>2+</sup> ions on the negative electrode.<sup>[3]</sup> Figure 4c presents the GCD curves of the ZIHCs with different molar ratios of HF hydrogel electrolytes under a current density of 0.5 mA cm<sup>-2</sup>. The non-ideal symmetric triangle further validated the hybrid energy storage mechanism of the ZIHCs. The CV curves at different scanning rates and GCD curves at different current densities for ZIHCs with different molar ratios of HF hydrogel electrolytes are shown in Figures S10–S13. The results indicated that the flexible ZIHCs could operate at high current densities. To verify the point, we also used a battery testing system to test the rate capability of the ZIHCs with different molar ratios of HF hydrogel electrolytes (Figure 4d). The ZIHC employing the HF<sub>16</sub> hydrogel electrolyte exhibited superior rate performance, maintaining 65% capacity ranging from 0.2 to 10 mA cm<sup>-2</sup>. Moreover, the cycling performance of the flexible ZIHC with the HF<sub>16</sub> hydrogel electrolyte was evaluated. As shown in Figure 4e, the flexible ZIHC still maintained a capacity retention rate of 87.7% after 1000 cycles, indicating that it had superior cycling stability.

As a potential application in wearable devices, ZIHCs will inevitably experience mechanical deformation, such as bending

and compression, during daily use.<sup>[40,41]</sup> Therefore, flexibility remains an essential characteristic of flexible ZIHCs. The electrochemical performance of the flexible ZIHC under different bending conditions was subsequently examined. After experiencing various bending angles, the capacitance of the flexible ZIHC barely deteriorated (Figure 4f), indicating its excellent flexibility. We also tested the capacitance retention and voltage output changes of the flexible ZIHC in different environments, such as bending, pressuring, puncturing, and cutting (Figure 4g). The capacitance of the flexible ZIHC showed minimal change after these operations, and the flexible ZIHC exhibited a similar voltage output to its initial flat state (Figure S14), confirming the excellent flexibility of the flexible ZIHC.

As a new type of antifreeze hydrogel electrolyte, the ion transport capacity at low temperatures is critical for ZIHCs. By testing the ionic conductivity of the HF<sub>16</sub> hydrogel electrolyte at low temperatures, we observed that it maintained a high ionic conductivity of 5.45 mS cm<sup>-1</sup> at -50 °C (Figure S15), which was conducive to the rapid transport of ions in the ZIHC. The superior ionic conductivity of hydrogel electrolyte at -50 °C originates from the hydrogen bond destruction effect of the hydrophilic units, the nano-confinement effect of the hydrophobic units, and the hydrogen bond destruction effect of the Zn(ClO<sub>4</sub>)<sub>2</sub> salt.<sup>[3,26,28]</sup> The low-temperature electrochemical performance of the flexible ZIHC was examined by CV and GCD. Figure 5a presents the CV curves of the ZIHC using the HF<sub>16</sub> hydrogel electrolyte under various operation temperatures at a scan rate of 0.5 mVs<sup>-1</sup>. We found that the flexible ZIHC still exhibited a current response, even at -50 °C, indicating that it could operate normally at this temperature. The GCD curves shown in Figure 5b confirmed that the flexible ZIHC could achieve normal operation at -50 °C. Compared with previous studies, our device achieved a lower operating temperature and higher capacity retention at -50 °C compared with most reported works (Table S1), demonstrating that the amphiphilic copolymer hydrogel electrolyte exhibited excellent low-temperature application potential. Figure 5c shows the rate performance of the flexible ZIHC at -50 °C. The device achieved a capacity retention rate of 26.3% in the current density range of 0.05–10 mA cm<sup>-2</sup>, exhibiting superior rate performance. Maintaining stable electrochemical performance after different temperature fluctuations is also crucial for low-temperature devices. Figure 5d shows the temperature fluctuation test results of the flexible ZIHC. After three temperature fluctuation test cycles, the flexible ZIHC could still maintain stable electrochemical performance. Moreover, the cyclic performance of the flexible ZIHC at low temperatures was evaluated. As shown in Figure 5e and S16, the flexible ZIHC maintained 95.5% of its capacity retention rate after 1500 cycles at -20 °C, and the capacity of the flexible ZIHC hardly declined after 2000 cycles at -50 °C, demonstrating excellent cycling performance. In addition, the application demonstrations at low temperatures demonstrated that the flexible ZIHC could offer broad potential for low-temperature applications (Figure 5f).

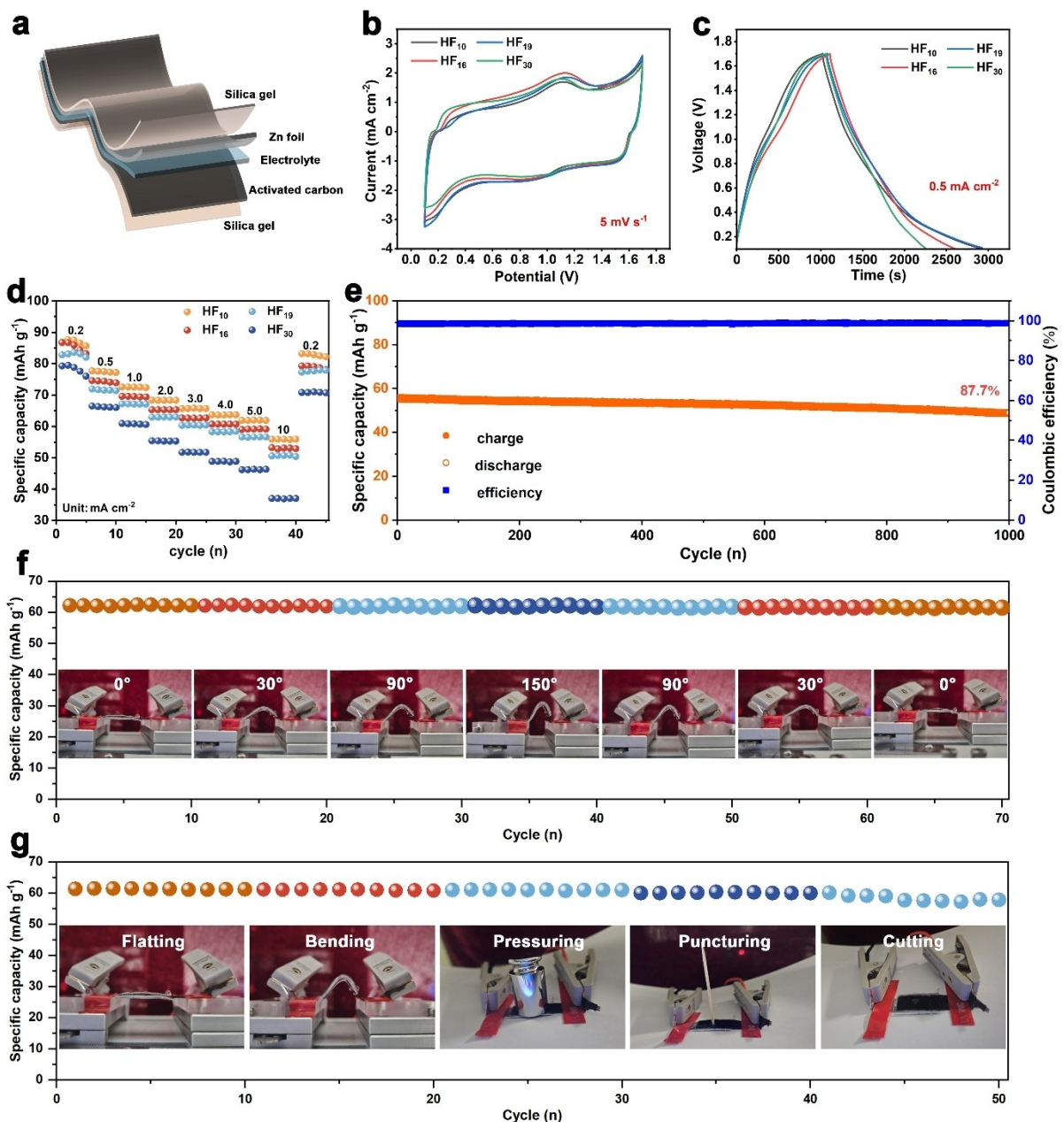


**Figure 4.** (a) Schematic diagram of the flexible ZIHC. (b) CV curves, (c) GCD curves, and (d) rate capability of flexible ZIHCs with different molar ratios of HF hydrogel electrolytes. (e) Room temperature cycling performance of the flexible ZIHC with the HF<sub>16</sub> hydrogel electrolyte. (f) Capacitance retention of flexible ZIHC at different bending angles. (g) Capacitance retention of flexible ZIHC under flatting, bending, pressuring, puncturing, and cutting.

## Conclusions

In summary, an amphiphilic copolymer hydrogel was synthesized through the polymerization of hydrophilic and hydrophobic monomers. The nano-confinement effect formed by the hydrophobic units and the hydrogen bond destruction effect of the hydrophilic units effectively reduced the number of strong hydrogen bonds, thereby lowering the freezing point of the hydrogel. The amphiphilic hydrogel also exhibited excellent adhesion performance, resulting in closer contact between the hydrogel electrolyte and the electrodes, effectively promoting the uniform deposition of  $\text{Zn}^{2+}$  ions and the rapid transport of

ions. In addition, the hydrogel electrolyte prepared by soaking the amphiphilic hydrogel in 1 M  $\text{Zn}(\text{ClO}_4)_2$  solution enabled the ZIHC to work normally at  $-50^\circ\text{C}$  and achieve superior low-temperature electrochemical performance. The application demonstration of the flexible ZIHC indicated that the device had great potential in wearable devices. This work offers a new strategy for the design of low-temperature hydrogel electrolytes for flexible electrochemical energy storage devices.

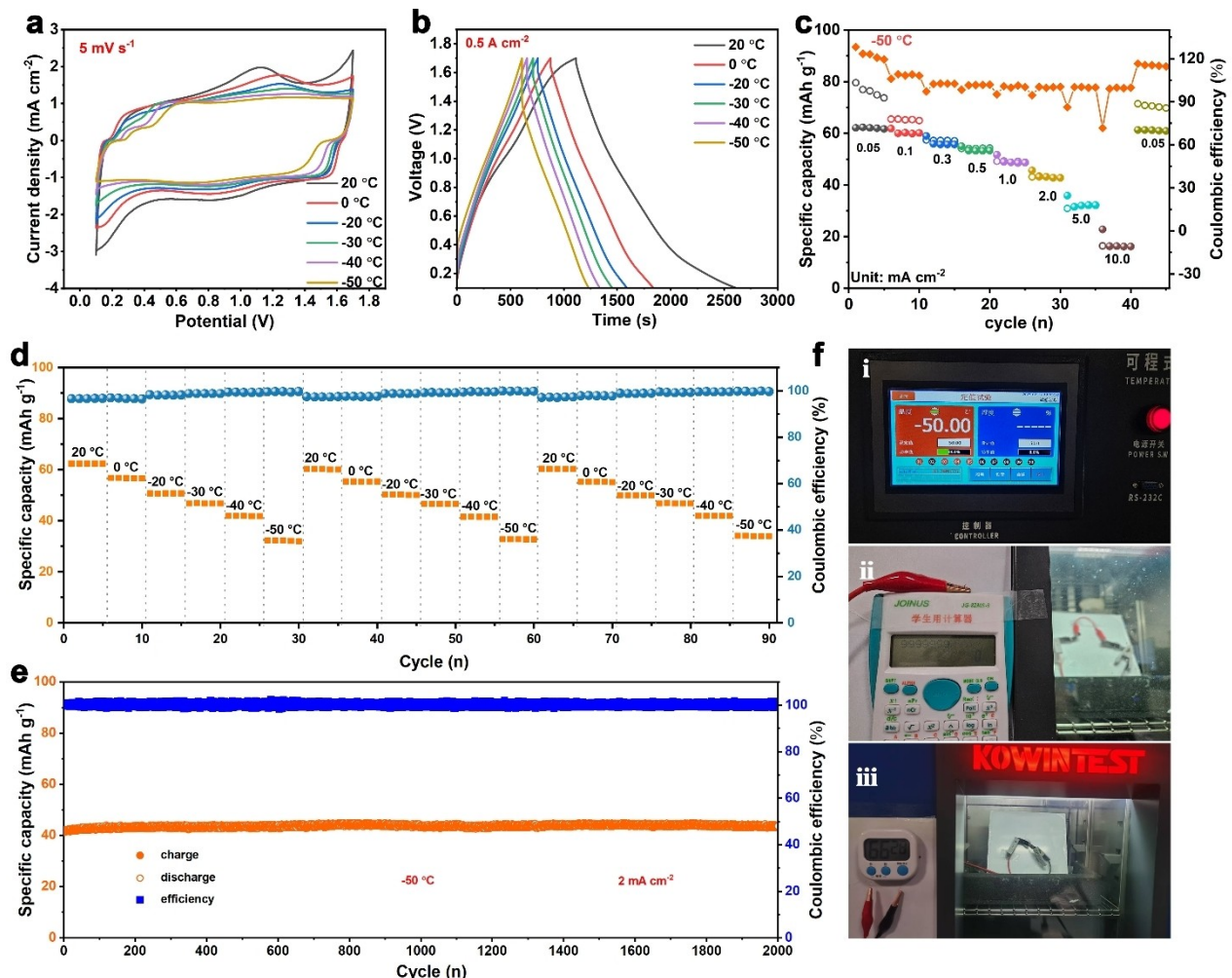


**Figure 5.** (a) CV curves and (b) GCD curves of the flexible ZIHC at various operating temperatures. (c) Rate capability of the flexible ZIHC at  $-50^{\circ}\text{C}$ . (d) Temperature fluctuation test for the flexible ZIHC. (e) Low-temperature cycling performance of the flexible ZIHC at  $-50^{\circ}\text{C}$ . (f) Low-temperature application demonstration of the flexible ZIHC.

## Experimental Section

### Materials

2-Hydroxyethyl acrylate (HEA, 99%) and 1H, 1H, 2H, 2H perfluorooctyl methacrylate (PFM, 98%) were obtained from Macklin, and both materials were used after removing the polymerization inhibitor through an alkaline alumina process. 2,2'-Azobis(2-methylpropionitrile) (AIBN,  $\geq 98\%$ ) was procured from Aladdin and used after recrystallization in ethanol. In addition, 1,4-dioxane ( $\geq 99.0\%$ ), N, N'-methylenebis (acrylamide) (MBAA, 99%), ammonium persulfate (APS,  $\geq 98\%$ ), and zinc perchlorate hexahydrate ( $\text{Zn}(\text{ClO}_4)_2 \cdot 6\text{H}_2\text{O}$ ) were obtained from Aladdin, Macklin, Sinopharm, and Alfa Aesar, respectively. Carbon cloth was procured from Cetech and activated with sulfuric acid and nitric acid before use.

### Synthesis of Copolymers

A specific molar ratio of HEA and PFM was mixed and stirred in 1,4-dioxane, and the solution was then purged with nitrogen for 1 h. Subsequently, AIBN was added and the solution was reacted at  $60^{\circ}\text{C}$  for 36 h, followed by cooling to room temperature. Petroleum

ether was added to precipitate the copolymer. The final precipitate was vacuum-dried at  $60^{\circ}\text{C}$  for 48 h to obtain the HF copolymer.

### Preparation of HF Hydrogel Electrolytes

The as-prepared dry HF copolymers were compressed into thin films using a plate vulcanizing apparatus at  $70^{\circ}\text{C}$  and 10 kPa. Then, the films were subsequently placed in a  $1\text{ mol kg}^{-1}$   $\text{Zn}(\text{ClO}_4)_2$  solution to swell, forming HF hydrogel electrolytes. Similarly, HF hydrogels were obtained by swelling the films in pure water.

### Preparation of chemically Cross-linked HEA Hydrogel Electrolyte

HEA was mixed with water, followed by the addition of APS and MBAA. The mixed solution was evenly stirred, followed by pouring the solution into a polytetrafluoroethylene (PTFE) mold. The mixture was then reacted at  $60^{\circ}\text{C}$  for 6 h to obtain the polymer. The chemically cross-linked HEA (XLHEA) hydrogel electrolyte was obtained by drying the polymer and allowing it to swell in a  $1\text{ mol kg}^{-1}$   $\text{Zn}(\text{ClO}_4)_2$  solution.

## Assembly of flexible Zinc Ion Hybrid Capacitor

For the positive electrode, a slurry was first obtained by mixing activated carbon (AC), acetylene black, and polytetrafluoroethylene binder at a ratio of 8:1:1. The solution was then coated on carbon cloth, with a load of 2 mg of active material per unit area. The Zn foil (0.03 mm) served as the negative electrode. A hydrogel electrolyte with a contact area of  $1\text{ cm}^{-2}$  was sandwiched between the positive and negative electrodes to assemble the ZIHC. The flexible ZIHC was subsequently encapsulated with Ecoflex 00-30 (Smooth-on).

## Material Characterization

Fourier transform infrared spectroscopy (INVENIO S, Bruker) was used to identify the functional groups and hydrogen bond distributions of the HF copolymers and hydrogels. Monomers or copolymers were dissolved in acetone-d6, and their composition was determined by  $^1\text{H}$  NMR spectroscopy (AVANCE 400, Bruker). The freezing point of the HF hydrogel was measured by a differential scanning calorimeter (DSC300, Netzsch), at a cooling rate of  $5\text{ K min}^{-1}$ . The surface morphologies of the dry hydrogel and Zn foil were observed by field emission scanning electron microscopy (Regulus 8100, Hitachi). X-ray diffraction (Smartlab SE, Rigaku) was used to characterize the crystal structure of the materials. The mechanical and adhesion properties of the hydrogels were measured by a universal testing machine (TSE104B, WANCE) at a rate of  $300\text{ mm min}^{-1}$ . In the adhesion test, the adhesion area was  $1\text{ cm}^2$ , and the following formula was used for calculating the adhesion strength:

$$T = F_{\max}/A \quad (1)$$

where T is the adhesion strength,  $F_{\max}$  denotes the maximum load at which the bonded joint fails, and A is the adhesion area.

The ionic conductivities of the hydrogels were measured by electrochemical impedance spectroscopy. The electrode consisted of stainless steel, and the hydrogel was sandwiched between the two electrodes. The ion conductivity was calculated by:

$$\sigma = L/RS \quad (2)$$

where L, R, S represent the thickness, Ohmic resistance and test area of the hydrogel, respectively.

## Electrochemical Measurements

The CV, GCD, CA, and corrosion tests were conducted using an electrochemical workstation (CHI660E). The CV values of the Zn//Cu asymmetrical cell were measured in a voltage window of  $-0.2$  to  $0.6\text{ V}$  at a scanning rate of  $5\text{ mVs}^{-1}$ . The CA curves were obtained based on the Zn//Zn symmetrical cell with an overpotential of  $-150\text{ mV}$  for  $200\text{ s}$ . The Tafel curve was measured in a voltage window of  $-0.2$  to  $0.2\text{ V}$ , at a scanning rate of  $1\text{ mVs}^{-1}$ . The Zn//Zn symmetric cells were assembled to test the cyclic performance of Zn plating/stripping. The Zn//Cu asymmetrical cells were subsequently used to test the Coulombic efficiency of Zn plating/stripping. The CV and GCD of the ZIHCs were measured at different scanning rates or current densities in a voltage window of  $0.1$ – $1.7\text{ V}$ , and the cycling performance of the ZIHCs was measured using a battery testing system (CT3002 A, LANHE). All low-temperature electrochemical tests were conducted in a temperature and humidity test chamber (Dongguan Kowin Testing Equipment Co.,

Ltd., China) or in an ultralow-temperature freezer (DW-HL100, Zhongke Meiling).

## Acknowledgements

This work was financially supported by the National Natural Science Foundation of China (22409126), Natural Science Foundation of Shandong Province (ZR2022QB014, ZR2024QF274, ZR2024QF281), Science and Technology Support Plan for Youth Innovation of Colleges and Universities of Shandong Province (2022KJ192), and Talent Introduction Project of Shandong First Medical University. We thank LetPub ([www letpub.com.cn](http://www letpub.com.cn)) for its linguistic assistance during the preparation of this manuscript.

## Conflict of Interests

The authors declare no conflict of interest.

## Data Availability Statement

The data that support the findings of this study are available from the corresponding author upon reasonable request.

**Keywords:** hydrogel electrolytes • flexible zinc-ion hybrid capacitors • amphiphilic copolymer hydrogels • low temperatures • intrinsic antifreeze

- [1] J. Zhu, J. Tai, T. Liu, Y. Wang, Y. Li, M. Yang, D. Ma, L. Deng, J. Luo, P. Zhang, *Adv. Energy Mater.* **2024**, 2403739.
- [2] Y. Sun, H. Ma, X. Zhang, B. Liu, L. Liu, X. Zhang, J. Feng, Q. Zhang, Y. Ding, B. Yang, L. Qu, X. Yan, *Adv. Funct. Mater.* **2021**, 31, 2101277.
- [3] Y. Sun, B. Liu, L. Liu, J. Lang, J. Qiu, *Small Struct.* **2023**, 4, 2200345.
- [4] R. Ma, Z. Xu, X. Wang, *Energy Environ. Mater.* **2023**, 6, e12464.
- [5] M. S. Javed, S. Asim, T. Najam, M. Khalid, I. Hussain, A. Ahmad, M. A. Assiri, W. Han, *Carbon Energy*. **2023**, 5, 271.
- [6] L. Miao, Y. Lv, D. Zhu, L. Li, L. Gan, M. Liu, *Chin. Chem. Lett.* **2023**, 34, 107784.
- [7] X. Ma, J. Cheng, L. Dong, W. Liu, J. Mou, L. Zhao, J. Wang, D. Ren, J. Wu, C. Xu, F. Kang, *Energy Storage Mater.* **2019**, 20, 335–342.
- [8] N. Piao, X. Gao, H. Yang, Z. Guo, G. Hu, H.-M. Cheng, F. Li, *eTransportation* **2022**, 11, 100145.
- [9] Y. Mu, F. Chu, B. Wang, T. Huang, Z. Ding, D. Ma, F. Liu, H. Liu, H. Wang, *InfoMat* **2024**, 6, e12611.
- [10] H. Wang, J. Liu, S. Ahmed, T. Wang, S. Song, *J. Energy Storage* **2022**, 56, 105923.
- [11] S. Huang, L. Hou, T. Li, Y. Jiao, P. Wu, *Adv. Mater.* **2022**, 34, 2110140.
- [12] Y. Zhao, Z. Chen, F. Mo, D. Wang, Y. Guo, Z. Liu, X. Li, Q. Li, G. Liang, C. Zhi, *Adv. Sci.* **2021**, 8, 2002590.
- [13] Y. Sun, L. Liu, X. Yan, *Adv. Funct. Mater.* **2022**, 32, 2109568.
- [14] Q. Liu, H. Zhang, J. Xie, X. Liu, X. Lu, *Carbon Energy*. **2020**, 2, 521–539.
- [15] C. You, W. Fan, X. Xiong, H. Yang, L. Fu, T. Wang, F. Wang, Z. Zhu, J. He, Y. Wu, *Adv. Funct. Mater.* **2024**, 34, 2403616.
- [16] E. Yang, X. Shi, L. Wu, H. Zhang, H. Lin, H. Liu, T. Bai, J. Qin, Y. Yu, S. Wang, Z.-S. Wu, *Adv. Funct. Mater.* **2024**, 34, 2313395.
- [17] M. Xu, B. Zhang, Y. Sang, D. Luo, R. Gao, Q. Ma, H. Dou, Z. Chen, *Energy Environ. Sci.* **2024**, 17, 8966.
- [18] K. Zhang, Y. Bai, L. Wang, Y. Gao, X. Li, X. Yang, W. Lü, *Langmuir* **2024**, 40, 26561–26569.
- [19] Z. Li, D. Chen, Y. An, C. Chen, L. Wu, Z. Chen, Y. Sun, X. Zhang, *Energy Storage Mater.* **2020**, 28, 307–314.

- [20] Q. Abbas, F. Béguin, *ChemSusChem* **2018**, *11*, 975–984.
- [21] G. Zhang, X. Yang, H. Shu, W. Zhong, *J. Mater. Chem. A* **2023**, *11*, 9097–9111.
- [22] G. Ji, R. Hu, Y. Wang, J. Zheng, *J. Energy Storage* **2022**, *46*, 103858.
- [23] Q. Zhang, Y. Ma, Y. Lu, L. Li, F. Wan, K. Zhang, J. Chen, *Nat. Commun.* **2020**, *11*, 4463.
- [24] W. Yi, S. Wu, Z. Zhou, X. Fang, X. Sun, J. Li, *ACS Appl. Energy Mater.* **2023**, *6*, 8838–8848.
- [25] Y. Sun, Y. Wang, L. Liu, B. Liu, Q. Zhang, D. Wu, H. Zhang, X. Yan, *J. Mater. Chem. A* **2020**, *8*, 17998.
- [26] Y. Sun, P. Ma, L. Liu, J. Chen, X. Zhang, J. Lang, X. Yan, *Sol. RRL* **2018**, *2*, 1800223.
- [27] C. G. Wiener, M. Tyagi, Y. Liu, R. A. Weiss, B. D. Vogt, *J. Phys. Chem. B* **2016**, *120*, 5543–5552.
- [28] C. Wang, C. G. Wiener, P. I. Sepulveda-Medina, C. Ye, D. S. Simmons, R. Li, M. Fukuto, R. A. Weiss, B. D. Vogt, *Chem. Mater.* **2019**, *31*, 135–145.
- [29] J. Madejová, M. Janek, P. Komadel, H.-J. Herbert, H. C. Moog, *Appl. Clay Sci.* **2002**, *20*, 255–271.
- [30] S. Ji, H. Luo, S. Qin, X. Zhang, Y. Hu, W. Zhang, J. Sun, J. Xu, H. Xie, Z. Yan, K. Yang, *Adv. Energy Mater.* **2024**, *14*, 2400063.
- [31] C. Jin, C. Yang, L. Xie, H. Mi, H. Yin, B. Xu, F. Guo, J. Qiu, *Adv. Energy Mater.* **2025**, *15*, 2402843.
- [32] Q. Fu, S. Hao, L. Meng, F. Xu, J. Yang, *ACS Nano* **2021**, *15*, 18469–18482.
- [33] Y. Yuan, J. Yang, Z. Liu, R. Tan, M. Chuai, J. Sun, Y. Xu, X. Zheng, M. Wang, T. Ahmad, N. Chen, Z. Zhu, K. Li, W. Chen, *Adv. Energy Mater.* **2022**, *12*, 2103705.
- [34] X. Zhang, J. Li, D. Liu, M. Liu, T. Zhou, K. Qi, L. Shi, Y. Zhu, Y. Qian, *Energy Environ. Sci.* **2021**, *14*, 3120.
- [35] L. Zhang, M. Lin, Z. Yu, Y. Huang, Q. Sun, X. Lu, H. Cheng, *Energy Storage Mater.* **2025**, 104022.
- [36] M. Wu, Y. Sun, Z. Yang, S. Deng, X. Nie, Y. Su, J. Li, G. Chai, *Angew. Chem., Int. Ed.* **2024**, e202407439.
- [37] D. Wang, D. Zhao, L. Chang, Y. Zhang, W. Wang, W. Zhang, Q. Zhu, *Energy Storage Mater.* **2025**, *74*, 103903.
- [38] S. Wang, L. Hu, X. Li, D. Qiu, S. Qiu, Q. Zhou, W. Deng, X. Lu, Z. Yang, M. Qiu, Y. Yu, *J. Energy Chem.* **2024**, *91*, 203–212.
- [39] Z. Zhou, X. Zhou, M. Zhang, S. Mu, Q. Liu, Y. Tang, *Small* **2020**, *16*, 2003174.
- [40] J. He, C. Lu, H. Jiang, F. Han, X. Shi, J. Wu, L. Wang, T. Chen, J. Wang, Y. Zhang, H. Yang, G. Zhang, X. Sun, B. Wang, P. Chen, Y. Wang, Y. Xia, H. Peng, *Nature* **2021**, *597*, 57.
- [41] Z. Liu, Z. Chen, S. Lei, B. Lu, S. Liang, J. Li, J. Zhou, *Adv. Mater.* **2024**, *36*, 2308836.

Manuscript received: January 14, 2025

Revised manuscript received: February 19, 2025

Accepted manuscript online: March 10, 2025

Version of record online: March 18, 2025